Theory of Plasmon-Assisted Transmission of Entangled Photons

Esteban Moreno,[1,*] F. J. García-Vidal,[2] Daniel Erni,[1] J. Ignacio Cirac,[3] and L. Martín-Moreno[4]

[1]*Swiss Federal Institute of Technology (ETH), IFH, ETH-Zentrum, CH-8092 Zurich, Switzerland*
[2]*Departamento de Física Teórica de la Materia Condensada, Universidad Autónoma de Madrid, E-28049 Madrid, Spain*
[3]*Max Planck Institut für Quantenoptik, Hans-Kopfermann Strasse 1, D-85748 Garching, Germany*
[4]*Departamento de Física de la Materia Condensada, Universidad de Zaragoza-CSIC, E-50009 Zaragoza, Spain*

(Received 13 August 2003; published 8 June 2004)

The recent surface plasmon entanglement experiment [E. Altewischer *et al.*, Nature (London) **418**, 304 (2002)] is theoretically analyzed. The entanglement preservation upon transmission in the non-focused case is found to provide information about the interaction of the biphoton and the metallic film. The entanglement degradation in the focused case is explained in the framework of a fully multimode model. This phenomenon is a consequence of the polarization-selective filtering behavior of the metallic nanostructured film. It is shown that the "which-way" labels that degrade entanglement are not located in the degrees of freedom of the metallic film but rather in the spatial degrees of freedom of the photon field.

DOI: 10.1103/PhysRevLett.92.236801 PACS numbers: 73.20.Mf, 03.67.Mn, 42.50.Dv

Entanglement is one of the strangest properties of quantum mechanics. Despite its puzzling character, this property, which is directly linked to the nonlocal nature of the theory, has been tested many times for simple systems. Recently, entanglement has started to be considered as a resource for applications in quantum information theory. This has driven the interest in the demonstration of entanglement for systems involving many particles. Large systems are more prone to decoherence processes, and, therefore, entanglement should be a very fragile property for them. For this reason the experiment showing plasmon-assisted transmission of entangled photons [1] has attracted quite a lot of interest. Some theoretical aspects of the experiment have been treated in Refs. [1,2], but a general (multimode) theory is still lacking. Here a complete detailed theory is derived and a thorough analysis addressing all aspects of the experiment is presented.

In Ref. [1], pairs of polarization-entangled photons are generated. The input biphoton state is a quasimonochromatic ($\lambda \simeq 813$ nm) quasiplane wave (propagating along the Z axis) in the polarization singlet $(|X_1 Y_2\rangle - |Y_1 X_2\rangle)/\sqrt{2}$ [X and Y denote horizontal and vertical polarization, respectively, and the subscripts ($i = 1, 2$) label the two photons]. After traveling along their respective trajectories parallel to the Z axis, photon i traverses polarizer P_i and is measured by detector D_i (the angle between the optic axis of P_i and the X axis is denoted β_i). These measured signals are combined to obtain the rate of coincident photon detections. Such a setup allows one to determine the biphoton fringe visibility V_{β_2} for fixed β_2, which is a measure of the photons' entanglement degree [3]. Photon 2 propagates freely from the source to P_2, whereas photon 1 traverses a 200 nm thick Au film deposited on top of a 0.5 mm glass substrate (Fig. 1). The metallic film is drilled with cylindrical holes (200 nm diameter) arranged as a square lattice (period 700 nm). The transmission of photon 1 through the subwavelength holes is mediated by surface plasmon modes [4,5]. The chosen wavelength corresponds (almost) to a transmission resonance ascribed to a surface mode at the metal-glass interface and propagating along the diagonals of the hole array, i.e., a $(\pm 1, \pm 1)$ mode. In order to investigate the effect of focusing on the entanglement of the output biphoton, the film is positioned at the focus of a confocal telescope in some parts of the experiment (lenses' focal length $f = 15$ mm, telescope's numerical aperture 0.13). Entanglement preservation upon transmission is reported when no telescope is used. The entanglement is, however, degraded when photon 1 is focused on the hole

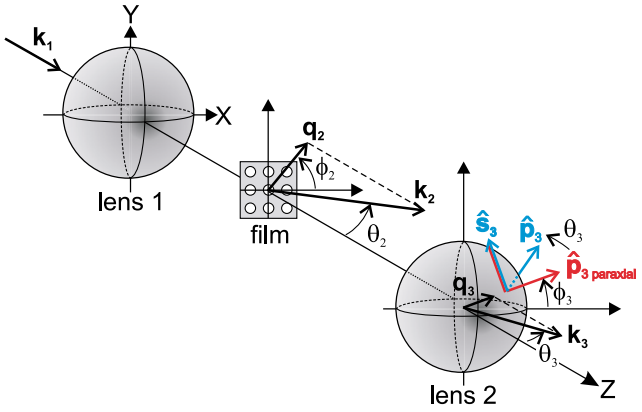

FIG. 1 (color online). Photon 1 trajectory. The confocal telescope (i.e., the lenses) is present only in some parts of the experiment. The incident photon is a plane wave with wave vector $\mathbf{k}_1 = (\mathbf{q}_1, k_{1z}) = (\mathbf{0}, k)$. The first lens produces a focused beam including many plane waves: $\mathbf{k}_2 = (\mathbf{q}_2, k_{2z})$. The second lens gives rise again to a bundle of modes: $\mathbf{k}_3 = (\mathbf{q}_3, k_{3z})$. The unit vectors $\hat{\mathbf{p}}_3$ and $\hat{\mathbf{s}}_3$ indicate the p and s polarization directions, respectively, whereas $\hat{\mathbf{p}}_{3\,\mathrm{paraxial}} = \hat{\mathbf{q}}_3$.

array and, moreover, the measured visibilities V_{0° and V_{45° are different.

Entanglement degradation is linked to the appearance of so-called "which-way" labels. Any degree of freedom of the systems interacting with the biphoton may become such a label. For this reason our model explicitly includes in the wave function all relevant degrees of freedom, i.e., not only the biphoton state but also the quantum state of the metallic film. When no telescope is used (monomode case), the initial global wave function (of the biphoton and solid) is $|\Phi_{\text{in}}\rangle = (|X_1Y_2\rangle - |Y_1X_2\rangle)/\sqrt{2} \otimes |S\rangle$, where $|S\rangle$ is the initial state of the solid. After photon 1 has traversed the hole array, the biphoton-film interaction finishes, and the global wave function $|\Phi_{\text{out}}\rangle$ can be written as

$$t_{X_1X_1}|X_1Y_2\rangle \otimes |S_{xx}\rangle + t_{Y_1X_1}|Y_1Y_2\rangle \otimes |S_{yx}\rangle - t_{X_1Y_1}|X_1X_2\rangle \otimes |S_{xy}\rangle - t_{Y_1Y_1}|Y_1X_2\rangle \otimes |S_{yy}\rangle, \quad (1)$$

where t_{AB} are the amplitudes of transmission through the film for the various channels, and $|S_{ab}\rangle$ are normalized wave functions for the final state of the solid. The system's final quantum state is defined by postselection, and for this reason $|\Phi_{\text{out}}\rangle$ includes only terms with exactly two photons. In other words, processes where, for instance, photon 1 is absorbed do indeed exist ($t_{0X_1}|0Y_2\rangle \otimes |S_{0x}\rangle - t_{0Y_1}|0X_2\rangle \otimes |S_{0y}\rangle$), but they are not relevant for the visibility measurement because only coincident photons are registered. Notice that the final states of the solid *must* be taken into account, as may be clearly seen by considering the two following extreme situations: (i) All $|S_{ab}\rangle$ are orthogonal to each other. In this case the solid and the biphoton can be entangled to a larger or lesser extent after the interaction (depending on the t_{AB} values), but the biphoton state (obtained by tracing the density matrix over the solid's degrees of freedom) is always a mixture of factorizable states and it is therefore completely disentangled [6]. Let us point out that in this case, after passage of photon 1, the solid incorporates "which-polarization" information linked to the photons' polarization state. This translates into an entanglement loss. (ii) All $|S_{ab}\rangle$ are equal. In this case the solid and the biphoton are completely disentangled after the interaction, and the biphoton state can range from factorizable to maximally entangled depending on the t_{AB} values. Since entanglement is preserved in some parts of Altewischer's experiment, (ii) is our model for the interaction process; i.e., the interaction does not introduce "which-way" labels in the solid. Such a theoretical framework explains why entanglement is preserved when the photon 1 is not focused. It is a simple consequence of two facts: first, no "which-way" labels are introduced in the solid, and, second, the transfer matrix t_{AB} for an orthogonally incident plane wave (nonfocused) on a square hole array is (by symmetry) proportional to the identity.

Within the present model the visibility computation requires only the determination of the transfer matrix $\mathbb{T}$ for the employed optical setup. When the telescope is used (to focus the field at a spot on the film), it is necessary to consider a multimode theory. The calculation proceeds as follows: (i) The electromagnetic field of photon 1 is expanded in plane waves $|\mathbf{q}\ \sigma\rangle$ before and after each optical element ($\sigma = \{p, s\}$ denotes the two possible polarizations; see Fig. 1). (ii) Lens and film are described by their transfer matrices in the aforementioned basis, $\mathbb{L}(\mathbf{q}_2, \mathbf{q}_1)$, $\mathbb{F}(\mathbf{q}_2)$, respectively. (iii) These matrices are combined to obtain the transfer matrix $\mathbb{T}(\mathbf{q}_3, \mathbf{q}_1)$ of the telescope with the hole array inside it. (iv) The biphoton transfer matrix $\mathbb{M}(\mathbf{q}_3, \mathbf{q}_1)$ for the whole setup (including polarizers) is then given by the tensor product of the transfer matrices for each photon, i.e., $\mathbb{M}(\mathbf{q}_3, \mathbf{q}_1) = \mathbb{P}_1(\mathbf{q}_3)\mathbb{T}(\mathbf{q}_3, \mathbf{q}_1) \otimes \mathbb{P}_2(\mathbf{0})$, where $\mathbb{P}_i$ are the polarizers' transfer matrices. In the case of normal incidence, the telescope plus hole array transfer matrix $\mathbb{T}(\mathbf{q}_3, \mathbf{0})$ turns out to be

$$\mathbb{R}(\phi_3) \int d\mathbf{q}_2 e^{i\frac{(n-1)\Delta}{2nk}(\mathbf{q}_2 - \frac{nf}{(n-1)\Delta}\mathbf{q}_3)^2} \mathbb{R}^{-1}(\phi_2)\mathbb{F}(\mathbf{q}_2)\mathbb{R}(\phi_2), \quad (2)$$

where $\mathbb{R}$ is the two-dimensional rotation matrix, n and Δ are the substrate refractive index and thickness, respectively ($n = 1.52$), k is the wave number, f is the focal length, and the remaining variables are explained in Fig. 1.

To obtain Eq. (2) a few approximations have been done. First, because of the low numerical aperture of the telescope, paraxial equations can be used. The lens transfer matrix $\mathbb{L}(\mathbf{q}_2, \mathbf{q}_1)$ is given by

$$\frac{f}{2\pi k i} e^{i\frac{f}{2k}(\mathbf{q}_2 - \mathbf{q}_1)^2} \mathbb{R}(\phi_2)\mathbb{R}^{-1}(\phi_1), \quad (3)$$

where the subscripts ($j = 1, 2$) refer to modes before and after the lens, respectively [Eq. (3) is obtained by means of a standard calculation in the paraxial regime but keeping the full vector character of the field]. Free propagation of a $|\mathbf{q}_2\ \sigma_2\rangle$ mode inside the telescope along a distance z amounts to an extra phase that, apart from global factors, is given by $\exp(-iz\mathbf{q}_2^2/2k)$ in the paraxial approximation. Second, the detectors are located at the back focal plane of an auxiliary lens placed after the polarizers. This implies that each point in the detector essentially collects one $|\mathbf{q}_3\rangle$ (in the limit of very large auxiliary lens aperture). For this reason the relative phases of the $|\mathbf{q}_3\rangle$ modes after the telescope are not relevant for the visibility computation. Third, concerning the hole array, again because of the low numerical aperture of the telescope, it is enough to keep the 0th diffracted order (higher orders are not collected by the second lens), and therefore the film transfer matrix $\mathbb{F}(\mathbf{q})$ is $\mathbf{q}$ diagonal. This matrix is

numerically computed as explained in [5]. Notice that, since the Au film is 200 nm thick, in our computations the gold permittivity is assumed to be local, and the nonlocal character of the surface plasmon arises as a consequence of its propagating nature. Figure 2 shows the computed transmittance when the hole array is illuminated by an orthogonally incident (nonfocused) plane wave, and the film is tilted around the diagonal [compare to Figs. 1(b) and 1(c) in [1]]. Despite the fact that the simulations do not exactly give the experimental peaks' height and width values, all main features are reproduced, including number and position of peaks, as well as overall order of magnitude. The behavior of the photonic bands as a function of parallel momentum is also correctly described.

The transfer matrix $\mathbb{T}(\mathbf{q}_3, \mathbf{0})$ corresponding to telescope plus film can be worked out analytically when $\mathbf{q}_3 = \mathbf{0}$, i.e., when the detector's aperture is extremely small. In this case the matrix before the integral in Eq. (2) disappears and the phase inside the integrand does not depend on ϕ_2. If one writes down explicitly $\mathbb{T}(\mathbf{0}, \mathbf{0})$ and takes into account the symmetry properties of the hole array, it can be shown that $\mathbb{T}(\mathbf{0}, \mathbf{0})$ is proportional to the identity [note that this result does not depend on the particular model for the numerical computation of $\mathbb{F}(\mathbf{q})$]. For this reason the whole setup should again preserve entanglement when only the following channels $(\mathbf{q}_1 = \mathbf{0}) \rightarrow (\text{all } \mathbf{q}_2) \rightarrow (\mathbf{q}_3 = \mathbf{0})$ are considered. This means that the focusing of photon 1 does not by itself degrade entanglement in every situation but, rather, only when the transfer matrix $\mathbb{T}$ is not proportional to the identity. This could be easily checked in an experiment by inserting an iris before the detector.

Figure 3 shows the visibilities obtained when the telescope is again employed, but now *all* channels $[(\mathbf{q}_1 = \mathbf{0}) \rightarrow (\text{all } \mathbf{q}_2) \rightarrow (\text{all } \mathbf{q}_3)]$ are considered. The visibility decreases as the telescope semiaperture increases (for 0° semiaperture the monomode case is obviously recovered). The same behavior observed in [1] for the $(\pm 1, \pm 1)$ mode is reproduced by the simulations for $\lambda = 797$ nm and telescope semiaperture 8°: $V_{45°} = 89\%$, $V_{0°} = 37\%$ (87 and 73 in the experiment, respectively). The numerical discrepancy for $V_{0°}$ can be essentially attributed to the fact that the computed transmission resonances are narrower than the measured ones, and the visibility is very sensitive to this variable. It is also to be noted that in [1] the employed wavelength is a bit larger than the resonant wavelength, whereas we have computed the visibility at the resonance maximum itself ($\lambda = 797$ nm). Our simulations show that $V_{0°}$ grows for wavelengths larger than the resonant one ($V_{0°} = 52\%$ for $\lambda = 802$ nm), whereas $V_{45°}$ remains approximately the same. Note that the visibilities are not monotone functions of the semiaperture. This is due to the fact that for larger semiapertures, higher values of θ_2 are included in the integral of Eq. (2), and this permits the excitation of surface modes different from $(\pm 1, \pm 1)$ (as can be indirectly seen in Fig. 2). The visibility reduction (as compared to the nonfocused case) can be understood because the transfer matrix $\mathbb{T}(\mathbf{q}_3, \mathbf{0})$ of the telescope plus film is not proportional to the identity anymore. This means that the system acts as a polarization-selective filter. The initial balance between the $|X_1 Y_2\rangle$ and $|Y_1 X_2\rangle$ components (which is responsible for the maximal entanglement of the input state) is therefore destroyed and, as a consequence, the entanglement is degraded. In the following it is explained why $V_{45°}$ and $V_{0°}$ behave differently.

Let us remember that, when V_{β_2} is measured, polarizer P_2 is set with this β_2. To understand the behavior of V_{β_2}

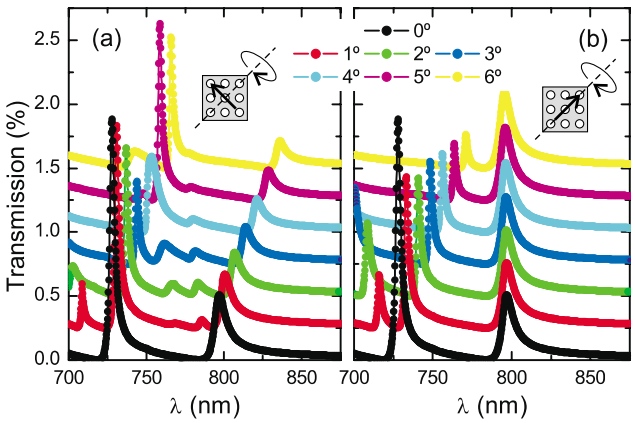

FIG. 2 (color). Hole array transmittance as a function of wavelength. The film is illuminated by an orthogonally incident plane wave (nonfocused), and it is tilted (from 0° to 6°) around the diagonal. The incident field linear polarization is perpendicular to the lattice diagonal in (a) and parallel to it in (b). For clarity the curves are offset 0.25%.

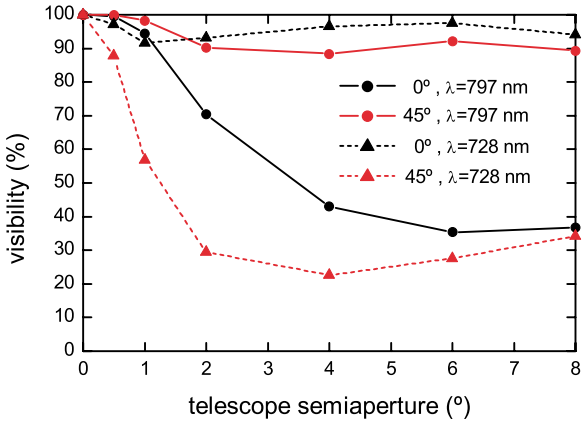

FIG. 3 (color online). Biphoton fringe visibility as a function of the telescope semiaperture. The visibilities are shown for two orientations of the second polarizer: $\beta_2 = 0°, 45°$. The chosen wavelengths are the resonances shown in Fig. 2 for no tilt: 797 nm (corresponding to a surface mode propagating along the array diagonals), and 728 nm (corresponding to a mode propagating along the X or Y axes).

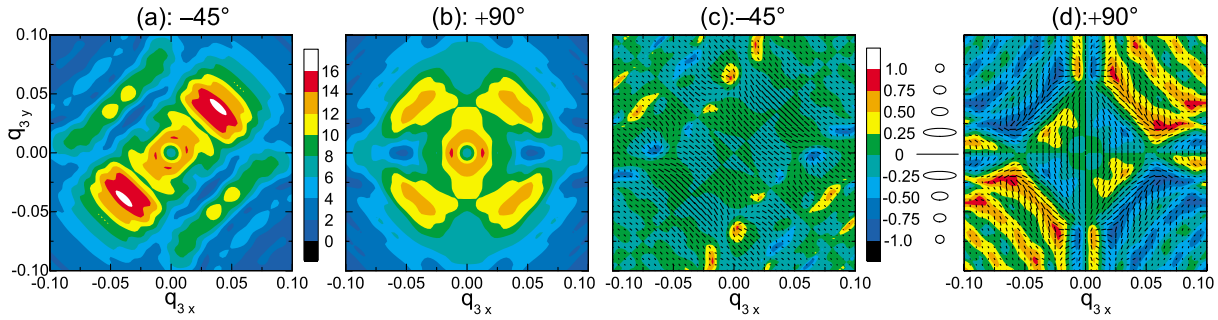

FIG. 4 (color). Intensities (a),(b) and polarizations (c),(d) of mode $|\mathbf{q}_3\rangle$ after the telescope as a function of (q_{3x}, q_{3y}). The excitation is one single linearly polarized photon ($\lambda = 797$ nm). The incident photon polarizations are $-45°$ in (a),(c) and 90° in (b),(d). The telescope semiaperture is 8°. The left color scale (arbitrary units) is shared by (a) and (b), and the right color scale corresponds to (c) and (d). In (c),(d) the color scale represents the ratio of the minor to the major polarization ellipse axes (for instance, ± 1 correspond to left and right circular polarization), and the small line segments indicate the orientation of the ellipse major axis. The maxima (and minima) of all abscissa and ordinate scales correspond to a semiaperture of $\theta_3 = 0.1°$.

one can plot the field after the telescope due to a single photon 1 incident with $\beta_2 + 90°$ linear polarization. This is so because the singlet biphoton state can be written as $(|\beta_2\ \beta_2 + 90°\rangle - |\beta_2 + 90°\ \beta_2\rangle)/\sqrt{2}$ for every β_2 (i.e., it is polarization isotropic). V_{β_2} will be 100% if there exists an orientation β_1 for polarizer P_1 that completely blocks the field due to photon 1 incident with linear polarization $\beta_2 + 90°$. Otherwise, as β_1 is varied, the collected intensity oscillates between a nonzero minimum and a maximum, and $V_{\beta_2} < 100\%$. Such polarization information is displayed in Fig. 4. Let us start with the analysis for $V_{45°}$. For $-45°$ incident polarization of photon 1, only the $(+1, -1)$ and $(-1, +1)$ modes are excited. The output field is predominantly linearly polarized along $-45°$ [Fig. 4(c)], yielding high $V_{45°}$ (a low photon coincidence rate will be registered for $\beta_1 = +45°$). On the other hand, the analysis for $V_{0°}$ is as follows. For 90° photon 1 incident polarization, all $(\pm 1, \pm 1)$ modes are excited, the output field is generally elliptically polarized [Fig. 4(d)], and it includes various polarization directions. This fact is responsible for the decrease in $V_{0°}$ (no β_1 exists that nearly blocks the field). Note that the central region of both diagrams is linearly polarized along the incident polarization direction. This fits with the transfer matrix being approximately proportional to the identity (for this region) and with the 100% visibility expected for small detector aperture, as discussed previously. It is also to be noticed that Figs. 4(a) and 4(b) compare well with Figs. 2b and 2d in [7] [as opposed to [7], circular fringes do not appear in Figs. 4(a) and 4(b) in the range shown because multiple interferences in the substrate were not included in the calculation]. The $\lambda = 728$ nm surface mode propagates at the air-metal interface along the $(\pm 1, 0)$ and $(0, \pm 1)$ directions and, as a consequence of previous discussion, the roles of $V_{45°}$ and $V_{0°}$ should be exchanged (this is, indeed, observed in the polarization diagrams for $\lambda = 728$ nm, not shown here for brevity). In fact, compared to $\lambda = 797$ nm, the high and low visibility values are now exchanged, as it is distinctly seen in Fig. 3, where $V_{45°}$ is low and $V_{0°}$ is high.

In conclusion, a detailed multimode theoretical analysis of the Altewischer *et al.* experiment has been presented. Entanglement preservation in the monomode case implies a particular model for the hole array-biphoton interaction; namely, this interaction does not introduce "which-way" labels in the metallic film. This is also the case when the photons are focused, as it is justified by the agreement between the measured visibilities and our numerical results. The "which-way" labels are therefore included in the spatial degrees of freedom of the first photon. The entanglement degradation is understood as a consequence of the polarization-selective filtering behavior of the hole array for nonorthogonal incidence. A polarization analysis explains the different values of the 0° and 45° visibilities.

Funded by the Swiss research initiative NCCR Quantum Photonics, and the Spanish MCyT under Contracts No. MAT2002-01534 and No. MAT2002-00139.

*Electronic address: esteban.moreno@uam.es

[1] E. Altewischer, M. P. van Exter, and J. P. Woerdman, Nature (London) **418**, 304 (2002).
[2] J. L. van Velsen, J. Tworzydlo, and C. W. J. Beenakker, Phys. Rev. A **68**, 043807 (2003).
[3] P. G. Kwiat *et al.*, Phys. Rev. Lett. **75**, 4337 (1995).
[4] T. W. Ebbesen *et al.*, Nature (London) **391**, 667 (1998).
[5] L. Martín-Moreno *et al.*, Phys. Rev. Lett. **86**, 1114 (2001).
[6] S. Hill and W. K. Wootters, Phys. Rev. Lett. **78**, 5022 (1997).
[7] E. Altewischer, M. P. van Exter, and J. P. Woerdman, J. Opt. Soc. Am. B **20**, 1927 (2003).